

# Vibrational Analysis of Mononitrosyl Complexes in Hemerythrin and Flavodiiron Proteins: Relevance to Detoxifying NO Reductase

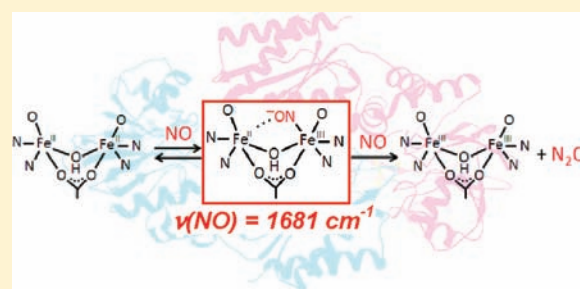
Takahiro Hayashi,<sup>†,‡</sup> Jonathan D. Caranto,<sup>§</sup> Hirotoshi Matsumura,<sup>†</sup> Donald M. Kurtz, Jr.,<sup>§</sup> and Pierre Moënne-Loccoz<sup>\*,†</sup>

<sup>†</sup>Division of Environmental and Biomolecular Systems, Institute of Environmental Health, Oregon Health and Science University, 20000 NW Walker Road, Beaverton, Oregon 97006-8921, United States

<sup>§</sup>Department of Chemistry, University of Texas at San Antonio, San Antonio, Texas 78249, United States

**S** Supporting Information

**ABSTRACT:** Flavodiiron proteins (FDPs) play important roles in the microbial nitrosative stress response in low-oxygen environments by reductively scavenging nitric oxide (NO). Recently, we showed that FMN-free diferrous FDP from *Thermotoga maritima* exposed to 1 equiv NO forms a stable diiron-mononitrosyl complex (deflavo-FDP(NO)) that can react further with NO to form N<sub>2</sub>O [Hayashi, T.; Caranto, J. D.; Wampler, D. A.; Kurtz, D. M., Jr.; Moënne-Loccoz, P. *Biochemistry* **2010**, *49*, 7040–7049]. Here we report resonance Raman and low-temperature photolysis FTIR data that better define the structure of this diiron-mononitrosyl complex. We first validate this approach using the stable diiron-mononitrosyl complex of hemerythrin, Hr(NO), for which we observe a  $\nu(\text{NO})$  at 1658 cm<sup>-1</sup>, the lowest  $\nu(\text{NO})$  ever reported for a nonheme {FeNO}<sup>7</sup> species. Both deflavo-FDP(NO) and the mononitrosyl adduct of the flavinated FDP (FDP(NO)) show  $\nu(\text{NO})$  at 1681 cm<sup>-1</sup>, which is also unusually low. These results indicate that, in Hr(NO) and FDP(NO), the coordinated NO is exceptionally electron rich, more closely approaching the Fe(III)(NO<sup>-</sup>) resonance structure. In the case of Hr(NO), this polarization may be promoted by steric enforcement of an unusually small FeNO angle, while in FDP(NO), the Fe(III)(NO<sup>-</sup>) structure may be due to a semibridging electrostatic interaction with the second Fe(II) ion. In Hr(NO), accessibility and steric constraints prevent further reaction of the diiron-mononitrosyl complex with NO, whereas in FDP(NO) the increased nucleophilicity of the nitrosyl group may promote attack by a second NO to produce N<sub>2</sub>O. This latter scenario is supported by theoretical modeling [Blomberg, L. M.; Blomberg, M. R.; Siegbahn, P. E. *J. Biol. Inorg. Chem.* **2007**, *12*, 79–89]. Published vibrational data on bioengineered models of denitrifying heme-nonheme NO reductases [Hayashi, T.; Miner, K. D.; Yeung, N.; Lin, Y.-W.; Lu, Y.; Moënne-Loccoz, P. *Biochemistry* **2011**, *50*, 5939–5947] support a similar mode of activation of a heme {FeNO}<sup>7</sup> species by the nearby nonheme Fe(II).



## INTRODUCTION

Flavodiiron proteins (FDPs) are widespread among microaerobic and anaerobic bacteria, archaea, and protozoan pathogens. Many FDPs provide protection against nitrosative stress by reductively scavenging NO to N<sub>2</sub>O.<sup>1–8</sup> This NO-reductase reaction occurs at a carboxylate-bridged nonheme diiron site proximal to a flavin mononucleotide (FMN) cofactor located across the homodimer subunit interface (Figure 1). In a previous study, we demonstrated that the diferrous site of an FMN-free FDP from *Thermotoga maritima* (*Tm* deflavo-FDP) (Figure 1) is capable of a single turnover of 2 NO to N<sub>2</sub>O in the presence of excess NO, albeit at a substoichiometric level since only ~0.7 equiv of N<sub>2</sub>O formed per deflavo-FDP diiron site.<sup>9</sup> In that same study, we further demonstrated that addition of one equiv NO per diferrous site results in essentially quantitative formation of a stable mononitrosyl adduct, which displays characteristic nitrosyl-to-iron LMCT absorptions at 420, 455, and 638 nm and a broad axial  $g \sim 2$  EPR signal only observable below 30 K. This EPR spectrum is clearly distinct from the  $g \approx 4$  resonances typically associated with nonheme  $S = 3/2$

{FeNO}<sup>7</sup> species.<sup>10</sup> Instead, the  $g \approx 2$  EPR signal is consistent with a ground-state  $S = 1/2$  system arising from antiferromagnetic coupling of an  $S = 3/2$  {FeNO}<sup>7</sup> with an  $S = 2$  high-spin Fe(II).<sup>9</sup> This description is reminiscent of that reported for the mononitrosyl adduct of the diferrous (deoxy) form of the O<sub>2</sub>-carrying nonheme diiron protein hemerythrin (Hr(NO)).<sup>11,12</sup> Relevant structural features of the Hr diiron site are included in Figure 1. Our results with *Tm* deflavo-FDP suggested a catalytic mechanism starting with the formation of the diiron-mononitrosyl adduct [Fe<sup>II</sup>·{FeNO}<sup>7</sup>], followed by the reaction of a second NO molecule to produce N<sub>2</sub>O and a diferric site. In the flavinated enzyme (FDP), the diferric site is then rereduced by the proximal FMNH<sub>2</sub> cofactor (Scheme 1).

Here, we report that the diiron-mononitrosyl complex is also observed in the flavinated enzyme, FDP(NO), and we further characterize this [Fe<sup>II</sup>·{FeNO}<sup>7</sup>] cluster using Fourier transform infrared spectroscopy (FTIR) spectroscopy. We also

Received: February 23, 2012

Published: March 26, 2012

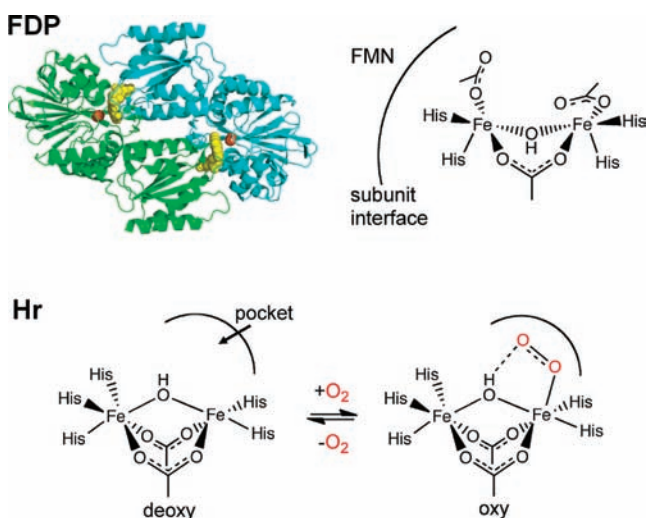


**Figure 1.** Backbone structure of *Tm* deflavo-FDP homodimer (green and blue ribbons, PDB entry 1VME). The iron atoms are depicted as orange spheres. Because a crystal structure of flavinated *Tm* FDP is not available, the FMN cofactor (yellow spheres) is from a backbone superposition of *Desulfovibrio gigas* FDP (PDB entry 1E5D).<sup>32</sup> Drawing generated in PyMOL (Delano Scientific, Inc.). Also shown as schematic structures of the consensus diiron site in FDPs (top right) and the diiron sites of diferrrous Hr and O<sub>2</sub> adduct of diferrrous Hr (deoxy and oxyHr, bottom schemes).

reexamine the vibrational spectra of Hr(NO), the only other known nonheme diiron-mononitrosyl complex. Previous resonance Raman (RR) studies of Hr(NO) identified the  $\nu(\text{FeNO})$  and  $\delta(\text{FeNO})$  modes from the  $\{\text{FeNO}\}^7$  chromophore but did not assign an N–O stretching vibration.<sup>11,12</sup> Our RR and FTIR experiments reveal that the  $[\text{Fe}^{\text{II}}\{\text{FeNO}\}^7]$  complexes in Hr(NO) and in FDP(NO) exhibit exceptionally low  $\nu(\text{NO})$  frequencies compared to those of  $\{\text{FeNO}\}^7$  species in other nonheme iron proteins and synthetic complexes.<sup>9,13</sup> Implications of these  $\nu(\text{NO})$  frequencies for the NO reduction mechanism of carboxylate-bridged diiron proteins are discussed.

## EXPERIMENTAL PROCEDURES

**Protein Preparations.** All protein concentrations are given in terms of nonheme diiron monomer. The expression and purification of recombinant *Phascolopsis gouldii* Hr was carried out as described previously.<sup>14</sup> <sup>13</sup>C-labeled Hr was expressed using the same procedure as that for unlabeled protein with minor modifications: a single colony of freshly transformed cells of the Hr overexpression strain<sup>14</sup> was cultured overnight in 50 mL of Luria–Bertani medium containing ampicillin. The cells were centrifuged at 4000 rpm for 10 min and resuspended and cultured in 1.0 L of M9 medium containing ampicillin and 3 g of [<sup>13</sup>C<sub>6</sub>]-D-glucose (99%, Cambridge Isotope Laboratories, Inc., Andover, MA) at 37 °C with shaking at 250 rpm. When the OD<sub>600</sub> of the culture reached ~0.6, IPTG was added to a final concentration of 0.5 mM to induce overexpression of the Hr gene. The induced culture was incubated for another ~3.5 h at the same temperature and shaking speed, and the cells were subsequently harvested by centrifugation at 4000 rpm for 20 min. Cell lysis and protein purification were carried out as described previously. The expression and purification

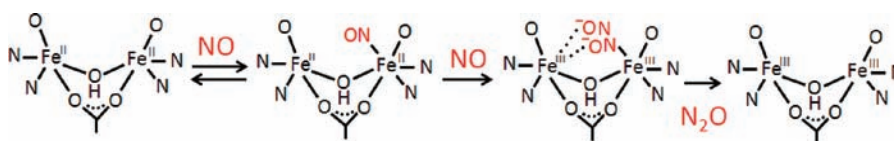
of recombinant *Tm* FDP, *Tm* rubredoxin (Rd), and *Tm* NADH: rubredoxin oxidoreductase (NROR) were performed as previously described.<sup>15</sup> *Tm* deflavo-FDP and the flavinated FDP were also prepared as described previously.<sup>9</sup>

**Preparation of NO Adducts.** All manipulations were conducted in an anaerobic glovebox containing <1 ppm of O<sub>2</sub> (Omnilab System, Vacuum Atmosphere Co.). Fully reduced (diferrrous) deflavo-FDP and Hr were obtained either by titration to achieve a slight stoichiometric excess of sodium dithionite or by addition of excess dithionite followed by removal of the reducing agent with a desalting spin column (Zebra, Pierce). Complete reduction of FDP was achieved by overnight incubation of ~100  $\mu\text{M}$  solutions in 50 mM 3-(*N*-morpholino)propanesulfonic acid (MOPS) pH 7.4, with 10 mM NADH, 4  $\mu\text{M}$  Rd and 0.4  $\mu\text{M}$  NROR; the excess NADH was removed after incubation using a desalting spin column inside the glovebox. Stoichiometric addition of NO to fully reduced proteins was achieved by adding small aliquots of NO-saturated aqueous solutions prepared from NO gas previously treated with 1 M KOH solution to remove higher nitrogen oxide impurities. The concentration of NO in the stock solutions was determined by titration against deoxymyoglobin. Alternatively, diethylammonium (*Z*)-1-(*N,N*-diethylamino)diazen-1-ium-1,2-diolate (diethylamine NONOate, Cayman Chemical, Ann Arbor, MI) was added to the reduced protein solutions. The concentration of the diethylamine NONOate stock solution was determined using an  $\epsilon_{250}$  of 6500 M<sup>-1</sup>cm<sup>-1</sup> in 0.01 M NaOH. Aliquot additions of diethylamine NONOate to a deoxymyoglobin control at pH ~5 were used to further confirm the concentration of NO produced. In both cases, these additions were made just prior to transfer into EPR tubes, Raman capillaries, or FTIR cells. Previously published UV–vis absorption spectra of Hr(NO)<sup>11,12</sup> and deflavo-FDP(NO)<sup>9</sup> were used to confirm the formation of the NO adducts.

**Molecular Spectroscopies.** Electronic absorption spectra were obtained using a Cary 50 Varian spectrophotometer. Low temperature FTIR photolysis was performed as previously described with slight modifications.<sup>9,16,17</sup> Approximately 15  $\mu\text{L}$  of ~1 mM protein solutions were deposited as a droplet on a CaF<sub>2</sub> window (International Crystal Laboratories, Garfield, NJ), and a second CaF<sub>2</sub> window was gently dropped on the sample to form an optical cell with a path length controlled by a 15- $\mu\text{m}$  Teflon spacer (International Crystal Laboratories, Garfield, NJ). After confirming the presence of the NO adduct by UV–vis absorption spectroscopy, the FTIR cell was mounted to a sample rod which was then flash-frozen in liquid N<sub>2</sub>, and inserted into the sample compartment of a closed-cycle cryogenic system (Omniplex, Advanced Research System).<sup>9,16,17</sup> This unit was placed inside the sample compartment of the FTIR and kept in the dark during the process of cooling to below 10 K. The temperature of the sample was monitored and controlled with a Cryo-Con 32 or a Lake Shore Model 331 unit. FTIR spectra were obtained on a Bruker Tensor 27 equipped with a liquid-N<sub>2</sub>-cooled MCT detector. Sets of 1000-scan accumulations were acquired at 4-cm<sup>-1</sup> resolution. Photolysis of nitrosyl complexes was performed by continuous illumination of the sample directly in the FTIR sample chamber using a 300-W arc lamp after filtering out heat and NIR emissions. The complete reversibility of all photolysis processes was confirmed by reproducing the same FTIR difference spectra after raising the sample temperature above 120 K, allowing rebinding of the photolyzed NO to the iron site.

Resonance Raman (RR) spectra were obtained on 1–2 mM protein solutions at either room temperature or 110 K using a custom McPherson 2061/207 spectrograph (set at 0.67 m with variable gratings) equipped with a liquid-N<sub>2</sub>-cooled CCD detector (LN-1100PB, Princeton Instruments). The 458- and 647-nm excitations were derived from an Ar laser (Innova 90, Coherent) and a Kr laser (Innova 302, Coherent),

## Scheme 1. Proposed Mechanism of NO Reduction in FDP



respectively. Long-pass filters (RazorEdge, Semrock) were used to attenuate Rayleigh scattering. To assess the photosensitivity of the NO adduct, rapid acquisitions with a range of laser power and continuous sample translation or rotation were compared with longer data acquisitions on static samples. Frequencies were calibrated relative to indene and aspirin standards and are accurate to  $\pm 1 \text{ cm}^{-1}$ . Polarization conditions were optimized using  $\text{CCl}_4$  and indene. The integrity of the RR samples was confirmed by direct monitoring of their UV–vis absorption spectra in Raman capillaries before and after laser exposure.

Electron paramagnetic resonance (EPR) spectra were obtained with a Bruker E500 X-band EPR spectrometer equipped with a superX microwave bridge and a dual-mode cavity with a helium flow cryostat (ESR900, Oxford Instrument, Inc.). The experimental conditions, that is, temperature, microwave power, and modulation amplitude, were varied to optimize the detection of all EPR-active species. Quantitation of the EPR signals was performed under nonsaturating conditions by double integration and comparison with a series of  $\text{Cu}^{\text{II}}$ EDTA standards at varying concentrations. Photolysis of samples was achieved by direct illumination of samples in the EPR cavity using the same 300-W arc lamp used in the FTIR photolysis experiments. Typical protein concentrations for the EPR experiments were  $\sim 100 \mu\text{M}$ .

## RESULTS

**Characterization of Hr(NO).** Technological improvements in RR and FTIR spectroscopies prompted us to reexamine the Hr(NO) complex in search of the  $\nu(\text{NO})$  mode, which was not detected in the previous RR study.<sup>12</sup> Using a 647-nm laser excitation on Hr(NO) samples kept at cryogenic temperatures, we were able to reproduce the resonance-enhanced bands at 434 and 421  $\text{cm}^{-1}$ , which in the previous study were assigned to  $\nu(\text{FeNO})$  and  $\delta(\text{FeNO})$  modes. Under these conditions, we also detect a band at 854  $\text{cm}^{-1}$  that downshifts with  $^{15}\text{NO}$  and  $^{15}\text{N}^{18}\text{O}$  (Figure S1, Supporting Information). We assign this latter band to a  $[\nu(\text{FeNO}) + \delta(\text{FeNO})]$  combination mode by analogy with similar RR vibrations in other nonheme  $\{\text{FeNO}\}^7$  complexes.<sup>9,13</sup> Detection of the  $\nu(\text{NO})$  mode requires data collection on samples at room temperature or with blue rather than red laser excitations (Figure S2, Supporting Information). The room temperature RR spectra of Hr(NO) obtained with a 458-nm excitation exhibit a band at 1671  $\text{cm}^{-1}$  that downshifts to 1647 and 1587  $\text{cm}^{-1}$  with  $^{15}\text{NO}$  and  $^{15}\text{N}^{18}\text{O}$ , respectively (Figure 2). While the  $-24 \text{ cm}^{-1}$  shift observed with  $^{15}\text{NO}$  is

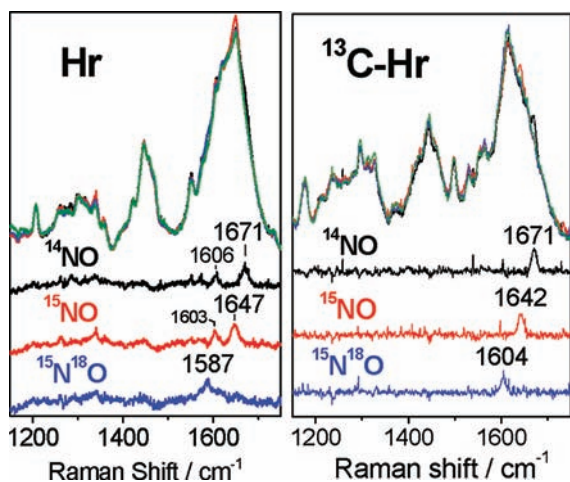


**Figure 2.** Room-temperature RR spectra of natural abundance and  $^{13}\text{C}$ -labeled deoxy-Hr (green) and their NO adducts prepared with  $^{14}\text{NO}$  (black),  $^{15}\text{NO}$  (red), and  $^{15}\text{N}^{18}\text{O}$  (blue) are superimposed above the corresponding NO adducts minus deoxy-Hr difference spectra. These spectra were obtained with a 458-nm laser excitation.

smaller than the  $-30 \text{ cm}^{-1}$  shift predicted for an isolated NO oscillator, the  $-84 \text{ cm}^{-1}$  shift observed with  $^{15}\text{N}^{18}\text{O}$  is larger than the  $-75 \text{ cm}^{-1}$  shift predicted by Hooke's law. These discrepancies between observed and calculated shifts, and in particular, a greater than expected isotope shift, are suggestive of Fermi coupling of the  $\nu(\text{NO})$  mode with another vibration(s). Accordingly, in the RR difference spectra obtained by subtracting the spectrum of deoxy-Hr from that of Hr(NO), the  $\nu(\text{NO})$  band is accompanied by a nearby signal at  $\sim 1606 \text{ cm}^{-1}$  (Figure 2). Based on FTIR data described below, this mode is assigned to a carboxylate  $\nu_{\text{as}}(\text{COO})$  mode. In agreement with this assignment, the Fermi coupling observed in the RR spectra of Hr(NO) is canceled by full  $^{13}\text{C}$ -labeling of Hr ( $^{13}\text{C}$ -Hr) since the  $\nu_{\text{as}}(^{13}\text{COO})$  downshifts away from the  $\nu(\text{NO})$  mode. Specifically, the RR spectrum of  $^{13}\text{C}$ -Hr(NO) shows an  $\nu(\text{NO})$  at 1671  $\text{cm}^{-1}$  that downshifts to 1642  $\text{cm}^{-1}$  with  $^{15}\text{NO}$ , as expected for an isolated NO diatomic oscillator (Figure 2). Low-temperature RR spectra of Hr(NO) show that the  $\nu(\text{NO})$  mode is significantly affected by temperature as it downshifts to 1661  $\text{cm}^{-1}$  at 110 K; in contrast, the  $\nu(\text{FeNO})$  and  $\delta(\text{FeNO})$  frequencies show only modest upshifts at cryogenic temperatures (Figure S2, Supporting Information).

As reported previously, Hr(NO) exhibits an axial  $S = 1/2$  EPR signal with  $g_{\parallel}$  and  $g_{\perp}$  near 2.78 and 1.80, respectively, arising from antiferromagnetic coupling between the  $S = 3/2$   $\{\text{FeNO}\}^7$  and the  $S = 2$  high-spin Fe(II).<sup>11,12</sup> Illumination of Hr(NO) at 4.2 K results in a loss of  $\sim 50\%$  of this EPR signal and in the appearance of a new resonance at  $g = 1.96$  characteristic of free NO (Figure 3). These light-induced EPR changes

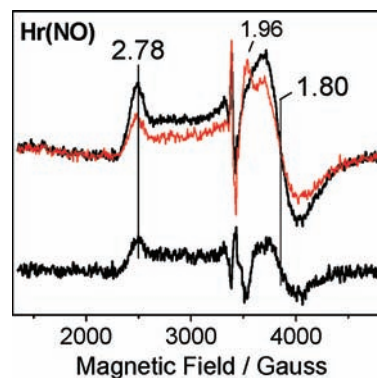


**Figure 3.** EPR spectra of Hr(NO) before (black) and after (red) illumination, and dark minus illuminated difference spectra (bottom trace), obtained at 4.2 K. Conditions: protein concentration, 60  $\mu\text{M}$  in 50 mM HEPES and 150 mM  $\text{Na}_2\text{SO}_4$  (pH 7.5); microwave frequency, 9.67 GHz; microwave power, 40  $\mu\text{W}$ ; modulation amplitude, 10 G.

are indicative of efficient photolysis of NO at cryogenic temperatures and are readily reverted by raising the sample temperature above 120 K to allow rebinding of NO at the diiron site.

Monitoring this photolysis process by FTIR spectroscopy using dark minus illuminated difference spectra reveals prominent positive bands at 1661, 1608, and 1398  $\text{cm}^{-1}$  and smaller perturbations across the spectral range (Figure 4). The double difference FTIR spectrum, computed from the light-induced difference spectra of Hr(NO) and Hr( $^{15}\text{NO}$ ), isolates isotope-sensitive modes and cancels out many light-induced differential signals (Figure 4). The remaining signals are (i) the positive band at 1661  $\text{cm}^{-1}$  that downshifts to 1637  $\text{cm}^{-1}$  with  $^{15}\text{NO}$ , assigned to the  $\nu(\text{NO})$  of the  $\{\text{FeNO}\}^7$  complex, (ii) a

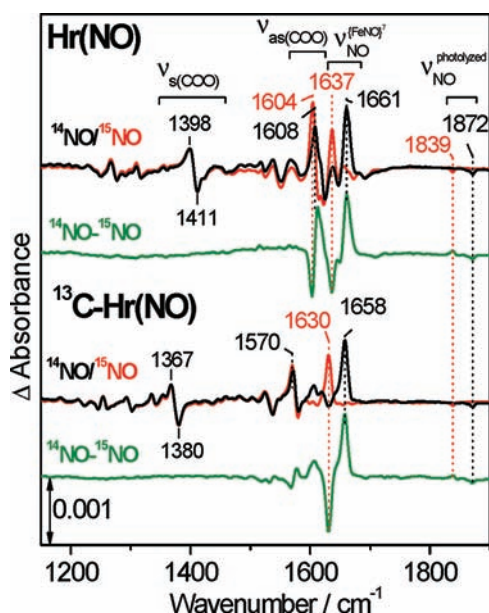


**Figure 4.** FTIR dark minus illuminated difference spectra of Hr(NO) (top) and  $^{13}\text{C}$ -Hr(NO) (bottom) with  $^{14}\text{NO}$  (black) and  $^{15}\text{NO}$  (red) at 20 K. Also shown are  $^{14}\text{NO}$  minus  $^{15}\text{NO}$  double-difference spectra (green).

weak negative band at  $1872\text{ cm}^{-1}$  that downshifts to  $1839\text{ cm}^{-1}$ , assigned to the  $\nu(\text{NO})$  of the photolyzed NO docked within the protein matrix, and (iii) the  $1608\text{ cm}^{-1}$  positive band that downshifts  $4\text{ cm}^{-1}$  to  $1604\text{ cm}^{-1}$ , assigned to a carboxylate  $\nu_{\text{as}}(\text{COO})$ . These assignments are also supported by FTIR spectra of Hr( $^{15}\text{N}^{18}\text{O}$ ) (Figure S3, Supporting Information) and by experiments using uniformly  $^{13}\text{C}$ -labeled Hr ( $^{13}\text{C}$ -Hr). Specifically, the differential signals at  $1608$  and  $1398\text{ cm}^{-1}$  in Hr(NO) downshift to  $1570$  and  $1367\text{ cm}^{-1}$  in  $^{13}\text{C}$ -Hr(NO) as expected for  $\nu_{\text{as}}(\text{COO})$  and  $\nu_{\text{s}}(\text{COO})$ , respectively, of a carboxylate group(s) (Figure 4). As the  $^{13}\text{C}$ -labeling downshifts the  $\nu_{\text{as}}(\text{COO})$ , it uncouples this mode from the  $\nu(\text{NO})$  of the  $\{\text{FeNO}\}^7$  species which is now observed at  $1658\text{ cm}^{-1}$  and exhibits a  $-28\text{ cm}^{-1}$  shift with  $^{15}\text{NO}$  in agreement with the calculated shift for an isolated diatomic oscillator. These FTIR results nicely support those from the RR spectra reported above. The frequency gap between  $\nu_{\text{as}}(\text{COO})$  and  $\nu_{\text{s}}(\text{COO})$ , denoted as  $\Delta_{\text{as-s}}$  is  $>200\text{ cm}^{-1}$  (Table 1). This  $\Delta_{\text{as-s}}$  value is consistent with  $\mu$ -1,3 bridging carboxylates,<sup>18,19</sup> which, based on the crystal structures of deoxy-Hr and its  $\text{O}_2$  adduct (Figure 1),<sup>20</sup> is the expected coordination geometry for the only two carboxylate ligands in Hr(NO). Although the previous RR investigation

reported that the  $\nu(\text{FeNO})$  and  $\delta(\text{FeNO})$  were sensitive to  $\text{H}_2\text{O}/\text{D}_2\text{O}$  exchange, we were not able to reproduce these observations in our RR spectra. Similarly, the FTIR spectra of Hr(NO) do not report any effect of H/D exchange on the  $\nu(\text{NO})$  mode (Figure S3, Supporting Information).

**Characterization of FDP(NO).** Addition of 1 equiv NO per diiron site to diferrous FDP or deflavo-FDP results in the formation of  $S = 1/2$   $[\text{Fe}^{\text{II}}\{\text{FeNO}\}^7]$  complexes with axial  $g \sim 2$  EPR signals (Figure 5). Double integration of these EPR signals against  $\text{Cu}^{\text{II}}\text{EDTA}$  standards indicates that they represent 0.8 spin per diiron site. While the EPR spectrum of FDP(NO) presents a well-resolved low-field resonance  $g_{\parallel}$  at 2.38 and a  $g_{\perp}$  at  $\sim 1.9$ , the spectrum of deflavo-FDP(NO) appears broader with a  $g_{\parallel}$  at 2.30 and  $g_{\perp}$  near 2.0. After illumination at low temperature, the EPR spectrum of FDP(NO) shows a large drop in the intensity of the low-field resonance at  $g = 2.38$ ; some unassigned signal appears to remain after illumination and new sharp EPR features appear, but these additional signals integrate to less than 10% of diiron sites (Figure 5). Although

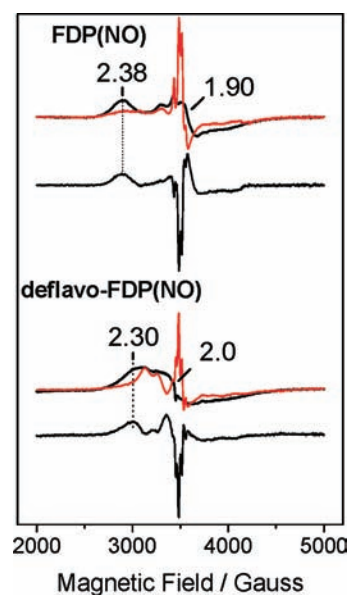


**Figure 5.** EPR spectra of FDP(NO) (top) and deflavo-FDP(NO) (bottom) before (black) and after (red) illumination at 4.2 K. Also shown below each pair are the resulting dark minus illuminated difference spectra. Conditions: protein concentration,  $100\text{ }\mu\text{M}$  in  $50\text{ mM}$  MOPS (pH7.4); microwave frequency,  $9.67\text{ GHz}$ ; microwave power,  $2\text{ mW}$ ; modulation amplitude of  $10\text{ G}$ .

**Table 1.** Vibrational Frequencies of  $S = 3/2$  Nonheme  $\{\text{FeNO}\}^7$  Species in Mono- and Dinuclear Complexes<sup>a</sup>

{FeNO} <sup>7</sup> species	$(\Delta^{15}\text{N})\text{ (cm}^{-1}\text{)}$		$(\Delta^{13}\text{C})\text{ (cm}^{-1}\text{)}$		$\Delta_{\text{as-s}}\text{ (cm}^{-1}\text{)}$	ref.
	$\nu(\text{Fe-NO})$	$\nu(\text{NO})$	$\nu_{\text{s}}(\text{COO-})$	$\nu_{\text{as}}(\text{COO-})$		
Hr(NO)	424 (-6)	1658 (-28) <sup>b</sup>	1398 (-31)	1608 (-38) <sup>b</sup>	203 <sup>b</sup>	This work
deflavo-FDP(NO) and FDP(NO)	451 (-9)	1681 (-29)	1421	1586	165	This work
deflavo-FDP(NO) <sub>2</sub>	459 (-7)	1749 (-30)				9
R2(NO) <sub>2</sub>	445 (-7)	1742 (-29)				13
SOR(NO)	475 (-7)	1721 (-31)				26
Fe(EDTA)(NO)	496 (-4)	1776 (-37)				9,10
Fe <sub>2</sub> (NO) <sub>2</sub> (Et-HPTB)(O <sub>2</sub> CPh) <sup>2+</sup>		1785 (-34)				24
Fe(NO)(S <sup>Me</sup> <sub>2</sub> N <sub>4</sub> (tren)) <sup>+</sup>		1685 (-45)				25

<sup>a</sup>R2 = ribonucleotide reductase R2 protein, SOR = superoxide reductase, EDTA = ethylenediamine tetra-acetate, Et-HPTB = *N,N,N',N'*-tetrakis(*N*-ethyl-2-benzimidazolyl-methyl)-1,3-diaminopropane, O<sub>2</sub>CPh = benzoate, S<sup>Me</sup><sub>2</sub>N<sub>4</sub>(tren) = 3-mercapto-3-methyl-2-butanone, tris(2-aminoethyl)amine.

<sup>b</sup>Based on FTIR frequencies obtained with  $^{13}\text{C}$ -Hr(NO).

illumination of deflavo-FDP(NO) also results in the loss of the  $g_{//}$  and  $g_{\perp}$  resonances, the EPR spectrum obtained after illumination displays more prominent features than in FDP(NO), and with the insight of the FTIR-photolysis data, these EPR data may reflect a greater heterogeneity in deflavo-FDP(NO).

As reported previously,<sup>9</sup> the RR spectrum of deflavo-FDP(NO) obtained with 458-nm excitation reveals a  $\nu(\text{FeNO})$  at  $451\text{ cm}^{-1}$ , but detecting the  $\nu(\text{NO})$  mode was precluded by the higher background signal observed in the high-frequency region.

The low-temperature dark minus illuminated FTIR difference spectrum of deflavo-FDP(NO) shows a positive band at  $1681\text{ cm}^{-1}$  that downshifts to  $1652\text{ cm}^{-1}$  with  $^{15}\text{NO}$  (Figure 6).

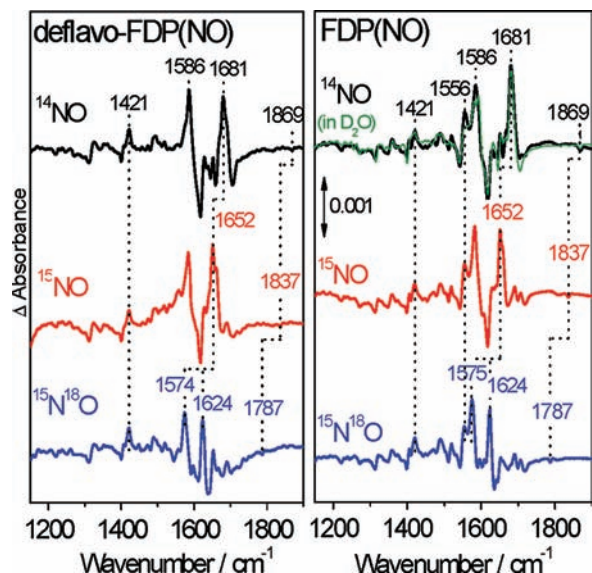


**Figure 6.** FTIR dark minus illuminated difference spectra of deflavo-FDP(NO) and FDP(NO) with  $^{14}\text{NO}$  (black),  $^{15}\text{NO}$  (red), and  $^{15}\text{N}^{18}\text{O}$  (blue) at 10 K.

Relatively intense differential signals centered at  $1586$  and  $1421\text{ cm}^{-1}$  are good candidates for the  $\nu_{\text{as}}(\text{COO})$  and  $\nu_{\text{s}}(\text{COO})$  of a bridging carboxylate group,<sup>18,19,21</sup> that is perturbed upon NO photolysis. As described for Hr(NO), the  $\Delta_{\text{as-s}}$  value of  $165\text{ cm}^{-1}$  suggests that these modes reflect perturbations of a bridging bidentate rather than terminal carboxylate ligand(s).<sup>22</sup> In deflavo-FDP( $^{15}\text{N}^{18}\text{O}$ ), the  $\nu(\text{NO})$  splits into two bands of equal intensity at  $1574$  and  $1624\text{ cm}^{-1}$ . The former frequency is below and the latter above the predicted  $1605\text{-cm}^{-1}$  value for a  $\nu(^{15}\text{N}^{18}\text{O})$  diatomic oscillator, suggesting Fermi coupling of this mode, presumably with an  $\nu_{\text{as}}(\text{COO})$  as in the vibrational spectra of Hr(NO). Negative  $\nu(\text{NO})$  bands from the photolyzed NO are very weak, but nevertheless, clearly identified, including in double difference FTIR spectra that combine photolysis and NO-isotopic sensitivity (Figure S4).

The light-induced FTIR difference spectra of FDP(NO) (Figure 6) are very similar to those of deflavo-FDP(NO), with positive and negative bands at  $1681$  and  $1869\text{ cm}^{-1}$ , respectively, and at  $1652$  and  $1837\text{ cm}^{-1}$  in FDP( $^{15}\text{NO}$ ). As with deflavo-FDP( $^{15}\text{N}^{18}\text{O}$ ), FDP( $^{15}\text{N}^{18}\text{O}$ ) exhibits a split  $\nu(^{15}\text{N}^{18}\text{O})$  at  $1575/1624\text{ cm}^{-1}$  compared to its predicted value of  $1605\text{ cm}^{-1}$  from Hooke's law. The differential signals assigned to  $\nu_{\text{as}}(\text{COO})$  and  $\nu_{\text{s}}(\text{COO})$  in the spectra of deflavo-FDP(NO), i.e.,  $1586$  and  $1421\text{ cm}^{-1}$ , respectively, are conserved in the spectra of FDP(NO). A shoulder at  $1556\text{ cm}^{-1}$ , which is not observed in the spectra of deflavo-FDP(NO) or in control experiments with

semi- or fully reduced FDP (Figure S5), does not shift with NO isotope labeling and is tentatively assigned to a perturbation of the FMN cofactor. As with Hr(NO), the  $\nu(\text{NO})$ s of deflavo- and FDP(NO) are not affected by H/D exchange (Figure 6), indicating that the bound NO group is not involved in hydrogen bond interactions.

## DISCUSSION

A striking observation from our results is that the  $[\text{Fe}^{\text{II}}\{\text{FeNO}\}^7]$  complexes of both Hr(NO) and FDP(NO) show  $\nu(\text{NO})$ s that are significantly lower than those of all previously reported nonheme  $\{\text{FeNO}\}^7$  species (Table 1 and Figure 7).

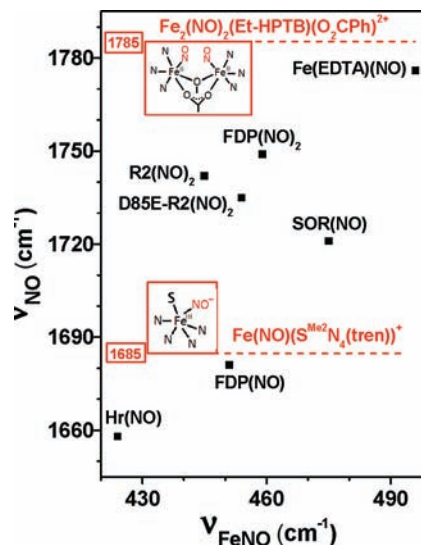


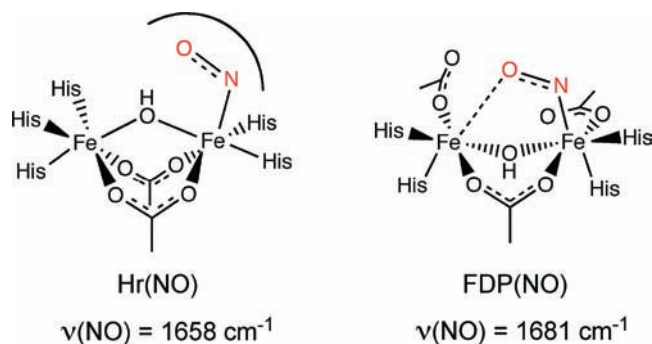
**Figure 7.**  $\nu(\text{FeNO})$  vs  $\nu(\text{NO})$  plot of  $S = 3/2$  nonheme  $\{\text{FeNO}\}^7$  complexes and proteins (see Table 1 for frequencies and references).

These low  $\nu(\text{NO})$ s suggest an unusually high  $\pi^*$  electron density at the nitrosyl group. The factors influencing the electronic distribution within nonheme  $S = 3/2$   $\{\text{FeNO}\}^7$  species between the limiting  $\text{Fe}(\text{I})(\text{NO}^+)$  and  $\text{Fe}(\text{III})(\text{NO}^-)$  formulations have been the subject of numerous studies.<sup>23</sup> Positively charged environments near the NO group, strong electron-donating ligands to the iron, and bent  $\text{Fe}-\text{N}-\text{O}$  unit can favor the  $\text{Fe}(\text{III})(\text{NO}^-)$  resonance structure. The only reasonably close structurally characterized mimic of the diiron-dinitrosyl coordination spheres in deflavo-FDP( $\text{NO}_2$ ) is  $\text{Fe}_2(\text{NO})_2(\text{Et-HPTB})(\text{O}_2\text{CPh})(\text{BF}_4)_2$ , where two equivalent  $S = 3/2$   $\{\text{FeNO}\}^7$  centers are in distorted octahedral coordination geometries with three N ligands and two O ligands from bridging  $\mu$ -alkoxo and  $\mu$ -carboxylate ligands. The crystalline complex has  $\text{FeNO}$  angles of  $167 \pm 1^\circ$ , and a single  $\nu(\text{NO})$  band at  $1785\text{ cm}^{-1}$ .<sup>24</sup> Both the  $\text{FeNO}$  angle and NO stretching frequency are at the higher end of the range observed for  $S = 3/2$   $\{\text{FeNO}\}^7$  units. In contrast, the 6-coordinate  $S = 3/2$   $\{\text{FeNO}\}^7$  unit in  $\text{Fe}(\text{S}^{\text{Me}_2}\text{N}_4(\text{tren}))(\text{NO})(\text{OTf})$  exhibits an  $\text{FeNO}$  angle of  $152^\circ$  and a  $\nu(\text{NO})$  at  $1685\text{ cm}^{-1}$ .<sup>25</sup> This  $100\text{-cm}^{-1}$  decrease in  $\nu(\text{NO})$  is believed to reflect the strong electron-donating character of the thiolate ligand which shifts electron density from the  $\text{Fe}-\text{NO}$  bond to the  $\pi^*$  N-O orbital. Similar notions of competition between  $\pi$  donating ligands were put forth by Johnson and co-workers<sup>26</sup> to explain the apparent weakening of the *trans*  $\text{Fe}-\text{S}(\text{Cys})$  bond in the NO adduct of superoxide reductase (SOR) compared to the oxidized (ferric) enzyme. Crystal structures of SOR suggest that the thiolate S atom acts as a hydrogen bond

acceptor, further weakening its electron-donation to the iron and allowing for strong electron-donation from the NO group in SOR(NO), as suggested by the high  $\nu(\text{NO})$  at  $1721\text{ cm}^{-1}$ .<sup>27</sup> Lehnert and co-workers observed a correlation between  $\nu(\text{FeNO})$  and  $\nu(\text{NO})$  in nonheme  $\{\text{FeNO}\}^7$  complexes with pyridyl, amine, and carboxylate ligands.<sup>28</sup> Their DFT calculations indicate that electron donation from anionic ligands inhibits  $\text{NO } \pi^* \rightarrow \text{Fe } d_{xz}$  and  $d_{yz}$  donation, thereby weakening both Fe–N and N–O bonds and lowering their corresponding stretching frequencies.

We, therefore, consider the possibility that the low  $\nu(\text{NO})$ s in Hr(NO) and FDP(NO) reflect an unusually strong competition for ligand-to-metal  $\pi$ -electron donation by the protein ligands. Based on crystal structures and the magnetic coupling of their iron centers,<sup>9,12,20</sup> the coordination spheres of the  $\{\text{FeNO}\}^7$  centers in Hr(NO) and FDP(NO) are expected to include two histidines, two carboxylate groups and a bridging solvent molecule, with the only apparent difference being a bridging versus terminal carboxylate ligand (Scheme 2).

**Scheme 2. Proposed structures of the diiron mononitrosyl clusters in Hr(NO) and FDP(NO)**



However, equivalent coordination spheres are also expected for the two  $\{\text{FeNO}\}^7$  units in deflavo-FDP(NO)<sub>2</sub> but they do not show unusually low  $\nu(\text{NO})$  (Table 1). The relatively carboxylate-rich diiron site expected in the dinitrosyl adduct of the R2 protein from *Escherichia coli* ribonucleotide reductase (R2(NO)<sub>2</sub>) also give rise to a "midrange"  $\nu(\text{NO})$  at  $1742\text{ cm}^{-1}$ .<sup>13</sup> The asymmetry of the diiron-mononitrosyl complexes in FDP(NO) and Hr(NO) relative to the diiron-dinitrosyl complexes in deflavo-FDP(NO)<sub>2</sub>, R2(NO)<sub>2</sub> and Fe<sub>2</sub>(NO)<sub>2</sub>(Et-HPTB)(O<sub>2</sub>CPh)<sub>2</sub>(BF<sub>4</sub>)<sub>2</sub> could conceivably allow electron donation from the Fe(II) center to the  $\{\text{FeNO}\}^7$  center. However, Mössbauer spectra of Hr(NO) show a clearly resolved ferrous signal with no evidence for unusual electron donation from the Fe(II) to the  $\{\text{FeNO}\}^7$  center.<sup>12,29</sup>

An alternative rationale may be that unusually small FeNO angles are stabilized in Hr(NO) and FDP(NO) because of steric constraints and semibridging electrostatic interactions between the  $\{\text{FeNO}\}^7$  and Fe(II) centers (Scheme 2), thereby favoring the Fe(III)(NO<sup>-</sup>) resonance structure and low  $\nu(\text{NO})$ s. In Hr(NO), NO is expected to bind to the same coordination site as does O<sub>2</sub> in oxyHr (Figure 1), and with six ligands to the Fe(II), five of which are from the protein, a semibridging NO coordination is not likely. However, a small FeNO angle could be enforced by the sterically confined pocket surrounding the O<sub>2</sub> coordination site.<sup>14,20</sup> Further bending of the FeNO unit upon thermal contraction of Hr(NO) may explain the  $10\text{-cm}^{-1}$  downshift of the  $\nu(\text{NO})$  mode at cryogenic temperatures. Hydrogen bonding between the bridging solvent and coordinated NO

could assist in stabilizing a small FeNO angle in Hr(NO) as occurs for coordinated O<sub>2</sub> in oxyHr. However, we could not detect a D<sub>2</sub>O-isotope effect in the vibrational spectra of Hr(NO).

In contrast to Hr, crystal structures of several FDPs<sup>6,7</sup> indicate a more expansive binding pocket near the diiron site, making steric restrictions on the FeNO angle less likely. The crystal structures also suggest that the Fe(II) center in FDP(NO) would retain an open coordination site and may permit a semibridging interaction of NO within the [Fe<sup>II</sup>•{FeNO}^7] unit. This type of interaction is, in fact, supported by DFT calculations.<sup>30</sup> The resulting electrostatic stabilization of electron density on the NO group of the  $\{\text{FeNO}\}^7$  unit could account for the low  $\nu(\text{NO})$ . This polarization toward the Fe(III)(NO<sup>-</sup>) resonance structure would also increase the nucleophilicity of the coordinated NO, thereby promoting its reactivity toward a second NO to form a hyponitrite intermediate (Scheme 1), as suggested by the aforementioned DFT calculations. In the case of Hr(NO), the steric restrictions enforcing the low FeNO angle would also inhibit interaction with a second NO. The extent to which the mononitrosyl-to-hyponitrite mechanism shown in Scheme 1 competes with binding of a second NO to the unoccupied Fe(II) in FDP(NO) to form a [ $\{\text{FeNO}\}^7$ ]<sub>2</sub> unit analogous to that in our previously characterized deflavo-FDP(NO)<sub>2</sub> is still unclear.<sup>9</sup> Interestingly, we also observed unusually low  $\nu(\text{NO})$ s in engineered myoglobins when the heme  $\{\text{FeNO}\}^7$  species is within a few angstroms from a distal nonheme iron(II) or Zn(II).<sup>31</sup> Asymmetric [Fe<sup>II</sup>•Fe<sup>III</sup>(NO<sup>-</sup>)] complexes may, thus, be common intermediates in the NO reductase activity of detoxifying, nonheme diiron, and denitrifying, heme-nonheme diiron enzymes.

## ■ ASSOCIATED CONTENT

### Supporting Information

Low-temperature RR spectra of <sup>13</sup>C-labeled deoxy-Hr and its NO-adduct obtained with 647- and 458-nm excitations, low-temperature FTIR difference spectra of Hr(NO), <sup>13</sup>C-Hr(NO), deflavo-FDP(NO), FDP(NO), semireduced and fully reduced FDP. This material is available free of charge via the Internet at <http://pubs.acs.org>.

## ■ AUTHOR INFORMATION

### Corresponding Author

\*Tel: 503-748-1673. Fax: 503-748-1464. E-mail: [plocco@ebs.ogi.edu](mailto:plocco@ebs.ogi.edu)

### Present Address

<sup>‡</sup>Department of Synthetic Chemistry and Biological Chemistry, Graduate School of Engineering, Kyoto University, Katsura, Kyoto 615-8510, Japan.

### Notes

The authors declare no competing financial interest.

## ■ ACKNOWLEDGMENTS

This article is dedicated to the memory of Thomas and Joann Loehr. This work was supported by the National Institute of Health (GM074785 to P.M.-L., GM040388 to D.M.K., and MBRS/RISE GM060655 to J.D.C.) and a Vertex Pharmaceutical Scholarship for T.H. We thank Dr. Michiko Nakano for help with the expression and purification of <sup>13</sup>C-Hr.

## ■ REFERENCES

- (1) Gardner, A. M.; Helmick, R. A.; Gardner, P. R. *J. Biol. Chem.* 2002, 277, 8172.

- (2) Gomes, C. M.; Giuffre, A.; Forte, E.; Vicente, J. B.; Saraiva, L. M.; Brunori, M.; Teixeira, M. *J. Biol. Chem.* **2002**, *277*, 25273.
- (3) Silaghi-Dumitrescu, R.; Coulter, E. D.; Das, A.; Ljungdahl, L. G.; Jameson, G. N.; Huynh, B. H.; Kurtz, D. M. Jr. *Biochemistry* **2003**, *42*, 2806.
- (4) Saraiva, L. M.; Vicente, J. B.; Teixeira, M. *Adv. Microb. Physiol.* **2004**, *49*, 77.
- (5) Silaghi-Dumitrescu, R.; Kurtz, D. M. Jr.; Ljungdahl, L. G.; Lanzilotta, W. N. *Biochemistry* **2005**, *44*, 6492.
- (6) Kurtz, D. M. J. *Dalton Trans.* **2007**, 4115.
- (7) Di Matteo, A.; Scandurra, F. M.; Testa, F.; Forte, E.; Sarti, P.; Brunori, M.; Giuffre, A. *J. Biol. Chem.* **2008**, *283*, 4061.
- (8) Le Fourn, C.; Brasseur, G.; Brochier-Armanet, C.; Pieulle, L.; Brioukhanov, A.; Ollivier, B.; Dolla, A. *Environ. Microbiol.* **2011**, *13*, 2132.
- (9) Hayashi, T.; Caranto, J. D.; Wampler, D. A.; Kurtz, D. M.; Moënne-Loccoz, P. *Biochemistry* **2010**, *49*, 7040.
- (10) Brown, C. A.; Pavlosky, M. A.; Westre, T. E.; Zhang, Y.; Hedman, B.; Hodgson, K. O.; Solomon, E. I. *J. Am. Chem. Soc.* **1995**, *117*, 715.
- (11) Nocek, J. M.; Kurtz, D. M. Jr.; Sage, J. T.; Debrunner, P. G.; Maroney, M. J.; Que, L. Jr. *J. Am. Chem. Soc.* **1985**, *107*, 3382.
- (12) Nocek, J. M.; Kurtz, D. M. Jr.; Sage, J. T.; Xia, Y. M.; Debrunner, P. G.; Shiemke, A. K.; Sanders-Loehr, J.; Loehr, T. M. *Biochemistry* **1988**, *27*, 1014.
- (13) Lu, S.; Libby, E.; Saleh, L.; Xing, G.; Bollinger, J. M.; Moënne-Loccoz, P. *J. Biol. Inorg. Chem.* **2004**, *9*, 818.
- (14) Farmer, C. S.; Kurtz, D. M. Jr.; Phillips, R. S.; Ai, J.; Sanders-Loehr, J. *J. Biol. Chem.* **2000**, *275*, 17043.
- (15) Hillmann, F.; Riebe, O.; Fischer, R. J.; Mot, A.; Caranto, J. D.; Kurtz, D. M. Jr.; Bahl, H. *FEBS Lett.* **2009**, *583*, 241.
- (16) Hayashi, T.; Lin, I. J.; Chen, Y.; Fee, J. A.; Moënne-Loccoz, P. *J. Am. Chem. Soc.* **2007**, *129*, 14952.
- (17) Hayashi, T.; Lin, M. T.; Ganesan, K.; Chen, Y.; Fee, J. A.; Gennis, R. B.; Moënne-Loccoz, P. *Biochemistry* **2009**, *48*, 883.
- (18) Costas, M.; Cady, C. W.; Kryatov, S. V.; Ray, M.; Ryan, M. J.; Rybak-Akimova, E. V.; Que, L. Jr. *Inorg. Chem.* **2003**, *42*, 7519.
- (19) Do, L. H.; Hayashi, T.; Moënne-Loccoz, P.; Lippard, S. J. *J. Am. Chem. Soc.* **2010**, *132*, 1273.
- (20) Stenkamp, R. E. *Chem. Rev.* **1994**, *94*, 715.
- (21) Duprat, A. F.; Traylor, T. G.; Wu, G. Z.; Coletta, M.; Sharma, V. S.; Walda, K. N.; Magde, D. *Biochemistry* **1995**, *34*, 2634.
- (22) Nara, M.; Tanokura, M. *Biochem. Biophys. Res. Commun.* **2008**, *369*, 225.
- (23) Sun, N.; Liu, L. V.; Dey, A.; Villar-Acevedo, G.; Kovacs, J. A.; Darensbourg, M. Y.; Hodgson, K. O.; Hedman, B.; Solomon, E. I. *Inorg. Chem.* **2010**, *50*, 427.
- (24) Feig, A. L.; Bautista, M. T.; Lippard, S. J. *Inorg. Chem.* **1996**, *35*, 6892.
- (25) Villar-Acevedo, G.; Nam, E.; Fitch, S.; Benedict, J.; Freudenthal, J.; Kaminsky, W.; Kovacs, J. A. *J. Am. Chem. Soc.* **2011**, *133*, 1419.
- (26) Clay, M. D.; Cosper, C. A.; Jenney, F. E. Jr.; Adams, M. W.; Johnson, M. K. *Proc. Natl. Acad. Sci. U.S.A.* **2003**, *100*, 3796.
- (27) Yeh, A. P.; Hu, Y.; Jenney, F. E. Jr.; Adams, M. W.; Rees, D. C. *Biochemistry* **2000**, *39*, 2499.
- (28) Berto, T. C.; Hoffman, M. B.; Murata, Y.; Landenberger, K. B.; Alp, E. E.; Zhao, J.; Lehnert, N. *J. Am. Chem. Soc.* **2011**, *133* (42), 16714.
- (29) Rodriguez, J. H.; Xia, Y.-M.; Debrunner, P. G. *J. Am. Chem. Soc.* **1999**, *121*, 7846.
- (30) Blomberg, L. M.; Blomberg, M. R.; Siegbahn, P. E. J. *Biol. Inorg. Chem.* **2007**, *12*, 79.
- (31) Hayashi, T.; Miner, K. D.; Yeung, N.; Lin, Y.-W.; Lu, Y.; Moënne-Loccoz, P. *Biochemistry* **2011**, *50*, 5939.
- (32) Frazao, C.; Silva, G.; Gomes, C. M.; Matias, P.; Coelho, R.; Sieker, L.; Macedo, S.; Liu, M. Y.; Oliveira, S.; Teixeira, M.; Xavier, A. V.; Rodrigues-Pousada, C.; Carrondo, M. A.; Le Gall, J. *Nat. Struct. Biol.* **2000**, *7*, 1041.